A Study of the Dynamics of Pd Oxidation and PdO Reduction by H_2 and CH_4

Stephen C. Su, Jason N. Carstens, and Alexis T. Bell

Chemical Sciences Division, Lawrence Berkeley Laboratory and Department of Chemical Engineering,
University of California, Berkeley, California 94720-1462

Palladium is one of the most active catalysts for the catalytic combustion of methane. Since Pd is oxidized during methane combustion to PdO and PdO is required for high activity, it is of interest to understand the dynamics of Pd oxidation and the structure of the oxide formed as well as the dynamics of PdO reduction by H_2 and CH_4. In the present study isothermal and temperature-programmed oxidation and reduction were used to probe the dynamics of the oxidation and reduction of zirconia-supported Pd. During uptake in oxygen, a monolayer of oxide is generated immediately, and upon further oxidation, the oxide forms a shell around a core of metal with thicknesses that increase with the oxidation temperature. The initial oxide is amorphous and subsequently transforms to crystalline PdO. The dynamics of Pd oxidation suggest that oxidation follows the Cabrera–Mott theory. Reduction of PdO by H_2 occurs in a shellwise manner, consistent with a shrinking core mechanism, while reduction in CH_4 occurs via an autocatalytic, nucleation mechanism. In the latter case, small particles of Pd must first be formed on which CH_4 can dissociate. The fragments (H and CH_x $(x = 3–1)$) diffuse to the metal–oxide boundary where reduction of the oxide occurs. Consistent with this picture, the kinetics of PdO reduction are first order in Pd initially, but then they become zero order in Pd. © 1998 Academic Press

INTRODUCTION

The catalytic combustion of methane is of current interest both as a means for generating power with minimal formation of NO and as a means for removing small amounts of methane from the emissions of methane-burning engines (see (1) and references cited therein). In the former case, the catalyst is operated at temperatures of up to 1073 K, while in the latter case, the catalyst must exhibit activity below 573 K. Of the various materials tested as catalysts, supported Pd has shown promise for both applications (1). In contrast to Pt, the activity of Pd is negligible unless it is oxidized; however, as little as four monolayer equivalents of PdO appear to be sufficient for the catalyst to achieve its full activity (2). What is not clear, though, is whether metallic Pd plays a role, even though PdO is essential. The present study was undertaken to determine the mechanism and dynamics of Pd oxidation and reduction. Oxidation and reduction of zirconia-supported Pd were carried out under both isothermal and temperature-programmed conditions, and the structure of the deposited oxide was characterized by Raman spectroscopy. A study of the factors affecting the oxidation of methane at low temperatures is presented in a related paper (3).

The oxidation of Pd has been studied on single crystals (4–14), foils (15, 16), and supported catalysts (2, 17, 18). It is generally believed that a monolayer of oxygen is rapidly adsorbed at temperatures above 200 K, the temperature for the onset of dissociative adsorption of O_2 on Pd (8), and that bulk oxidation begins above 473 K. Studies conducted on Pd(100) (4) and Pd(111) (10, 12, 14) suggest the formation of a suboxide which acts as a precursor to bulk oxidation. Penetration of the oxidation front into the bulk is thought to begin at nucleation or defect sites (12), and it has been proposed (7) that during the early stages of bulk oxidation, crystalline PdO at the nucleation sites expands to form a coherent oxide layer.

PdO reduction by H_2 has been investigated by several authors (19–22). The reduction of oxygen adsorbed on Pd(111) occurs by a Langmuir–Hinshelwood mechanism (20). The rate-limiting step is thought to be the reaction between adsorbed H and adsorbed O, as the subsequent reaction between adsorbed H and adsorbed OH to form water is fast. Reduction of PdO in CH_4 has not been as well characterized as reduction in H_2. Temperature-programmed reduction of supported PdO shows that reduction occurs above 423 K (23, 24). In studies conducted with a fully oxidized Pd foil it was found that reduction nucleated at the edge of the foil and then moved as a front across the surface of the oxide (25). Several authors have suggested that the first step in the reduction of PdO by methane is the dissociative adsorption of CH_4 (1). However, while methane is known to adsorb dissociatively on supported and unsupported Pd metal (26), it does not adsorb on oxygen-covered Pd (27). In fact, methane adsorption on Pd(110) has been found to decrease linearly with increasing oxygen coverage with each oxygen atom blocking two active sites on which
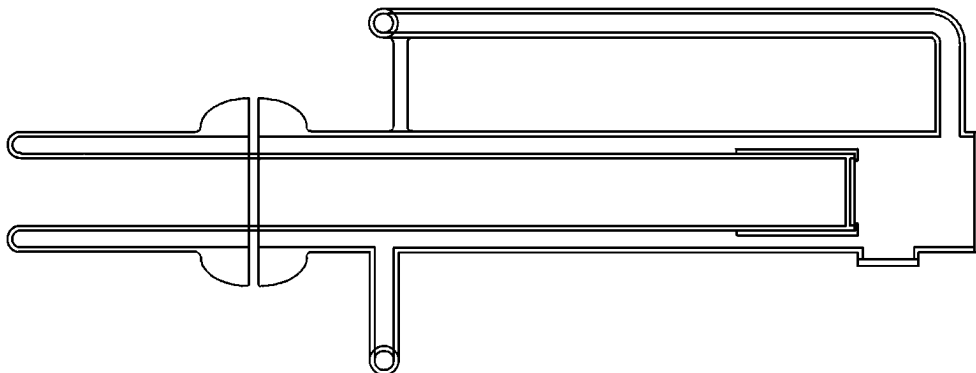
FIG. 1.   Schematic diagram of the *in situ* Raman cell.

methane can adsorb. Therefore, there is some question as to whether metallic Pd is necessary to nucleate the reduction of PdO by CH_4.

EXPERIMENTAL

The 9.91 wt% Pd/ZrO_2 was obtained from Catalytica. This catalyst was prepared by incipient wetness impregnation of zirconia with a solution of palladium nitrate. The catalyst was then air dried and calcined at 773 K for an extended period in pure O_2.

For the constant-temperature and temperature-programmed experiments using mass spectrometry, a 20 cm long quartz microreactor with a 0.9 cm ID quartz frit was used to support 0.272 g of catalyst. A thermocouple was placed into the catalyst bed for temperature measurements. The reactor was placed inside an electrically heated furnace controlled by a programmable temperature controller (Omega Series CN-2010). He (99.999% Bay Airgas), H_2 (99.9999%, Air Products), CH_4 (99.97%, Matheson), and O_2 (99.999%, Air Products) were supplied to the reactor from a gas manifold. A mass flow controller (TYLAN FC-280) controlled the flow rate of each gas. A six-way valve, located approximately 60 cm upstream of the catalyst bed was used to inject pulses of either hydrogen or methane into the carrier gas.

The reactor effluent was monitored by a UTI Model 100C quadrupole mass spectrometer interfaced to a personal computer (Gateway 2000 4DX-33) for data acquisition. A portion of the effluent from the reactor was introduced through a leak valve (Granville-Phillips Series 203) into the vacuum chamber containing the mass spectrometer detector. Data points were taken every second during titration experiments and every 10 s during temperature-programmed experiments. The signal from the mass spectrometer was calibrated using appropriate calibration gases.

Immediately downstream of the six-way valve used to inject pulses into the carrier gas was a four-way valve. This valve allows carrier gas, which normally flows through the reactor, to bypass the reactor and, hence, isolate the reactor

from the rest of the flow system. In this way, injected gases could be passed either through the reactor or diverted via the bypass.

For Raman studies, 0.442 g of the air-calcined powder was pressed into a pellet (10,000 psi). The pellet was placed in a quartz Raman cell (Fig. 1). The cell consists of a 1 in. OD quartz tube with two Heraeus Amersil Suprasil 311 quartz optical windows. The scattered light is collected with a Nikon Nikkor F 50 mm f/1.2 camera lens. The cell is heated with two 150 W semi-cylindrical radiant ceramic heaters (Omega, HSK-10665). Spectra were acquired using a Spex double monochromator operated as a spectrophotometer. A laser line interference filter (Oriel Model 52660) was used to remove plasma light from the laser. A single-notch holographic filter (Kaiser Optical HNF-514.5-1.0) was used to eliminate Rayleigh scattering, and the signal was detected by a photodiode array (Princeton Instruments EIRY-1024). The Raman spectra were recorded with a spectral resolution of 1.8 cm^{-1} and calibrated using a neon lamp. The 514.5 nm line of an argon ion laser was used and the laser power at the sample was set at 150 mW. Peak shifting due to laser heating was not observed when the power was varied between 60 and 150 mW. The gas chromatograph (SRI 8610B) uses an Alltech CTR I column that can separate CO_2, O_2, N_2, CH_4, and CO. The column is operated at 323 K and a carrier gas flow rate of 60 cm^3/min, giving an elution time of 9 min.

All experiments were performed with the catalyst first pretreated at 773 K for 2 h in pure O_2 (1 atm) flowing at 60 cm^3/min followed by reduction for 1 h in 25% H_2 in He (1 atm) flowing at 60 cm^3/min. In cases where the catalyst was prereduced, the catalyst was then cooled to the reaction temperature, purged with He, and exposed to a reaction mixture of 3% CH_4/5% O_2 in He (1 atm). In cases where the catalyst was preoxidized, the catalyst was cooled to the appropriate preoxidation temperature and exposed to pure O_2 (1 atm) flowing at 60 cm^3/min for 1 h. The catalyst was then cooled to the reaction temperature, purged with He, and exposed to the reaction mixture. Temperature programmed oxidation with O_2 was performed by ramping

the sample temperature from 298 to 673 K at 10 K/min in 0.4% O_2 in He (1 atm) flowing at 60 cm^3/min. Unconsumed O_2 was measured using a mass spectrometer. Temperature-programmed reduction with CH_4 was performed by ramping the sample temperature from 298 to 778 K at 10 K/min in 3% CH_4 in He (1 atm) flowing at 60 cm^3/min unless otherwise noted. CO_2 produced was measured using a mass spectrometer. The absence of any signal intensity for mass 28 above that due to the cracking of CO_2 was used to conclude that CO was not produced. This conclusion was confirmed by checking the oxygen mass balance for experiments involving the oxidation and reduction of Pd.

RESULTS AND DISCUSSION

The catalyst was characterized in its fully reduced state to determine the dispersion of Pd and in its fully oxidized state to determine the structure of the oxide phase. The dispersion of the reduced catalyst was measured using the method of Benson *et al.* (28). The catalyst was first reduced in a stream of 25% H_2 in He for 1 h at 373 K. After purging in He, the catalyst was exposed for 30 min at 373 K to a 1 atm stream containing 32% O_2 in He flowing at 60 cm^3/min. The oxygen accumulated on the Pd surface was removed by passing pulses of 20% H_2 in He (1 atm) through the catalyst at 1-min intervals while the catalyst was maintained at 373 K. This procedure was continued until no more H_2 consumption was observed. The moles of H_2 consumed were used to calculate the amount of exposed Pd assuming the stoichiometry $PdO + 1.5 H_2 \rightarrow PdH + H_2O$. By this means, the catalyst was found to contain 37.9 μmol of surface Pd per gram of catalyst, which corresponds to a Pd dispersion of 4%. For the mass of catalyst used in the present experiments, 0.272 g, and the measured dispersion, one monolayer is equivalent to 10.3 μmol of Pd or PdO and, correspondingly, a fully oxidized sample contains 24.8 ML equivalents of oxide. Assuming spherical crystallites, the average particle diameter is estimated to be 28 nm.

Following H_2–O_2 titration, temperature-programmed desorption of H_2 was carried out by ramping the temperature at 10 K/min in He flowing at 60 cm^3/min. Hydrogen desorption was observed between 400 and 800 K, with the amount of H_2 desorbed corresponding very closely to that expected on the basis of reaction stoichiometry given above for H_2/O_2 titration.

Fully reduced ZrO_2-supported Pd was oxidized to PdO by exposing the catalyst to 1 atm of O_2 flowing at 60 cm^3/min for 1 h at 773 K. Subsequent reduction of the oxidized sample indicates that it contains the stoichiometric amount of oxygen expected for PdO. A Raman spectrum of the fully oxidized sample recorded at 298 K is shown in Fig. 2 The intense band at 651 cm^{-1}, as well as the weaker bands at 425, 445, 725, 935, and 1051 cm^{-1} are all characteristic of bulk, crystalline PdO (29, 30). Upon reduction of the sample in H_2, all of the features observed in Fig. 2 disappear,
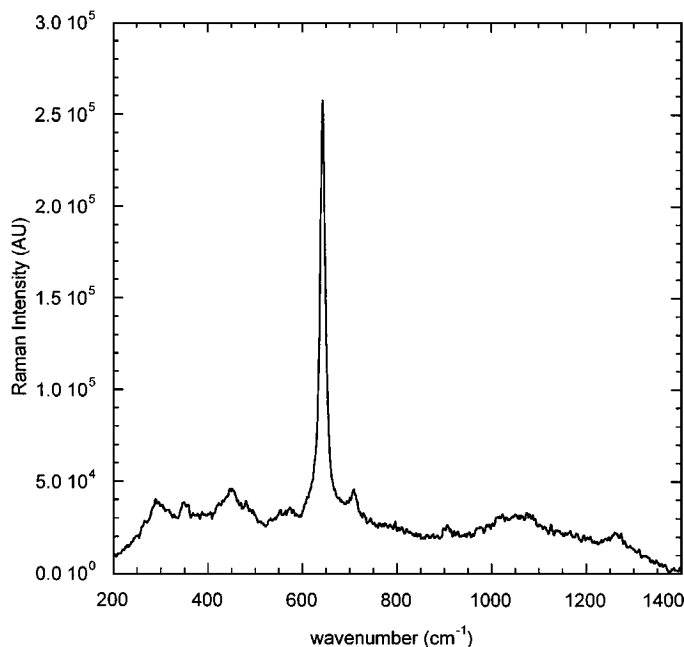
FIG. 2. Raman spectrum of 10 wt% Pd/ZrO$_2$ at 298 K after oxidation in 1 atm O$_2$ at 773 K for 1 h.

and only weak features characteristic of the monoclinic and cubic phases of ZrO_2 are visible.

The temperature range over which the oxidation of Pd/ZrO_2 occurs was determined by TPO. A mixture of 0.4% O_2 in He flowing at 60 cm^3/min was passed over the sample while the temperature was raised from 298 to 800 K at 10 K/min. Figure 3 shows the TPO spectrum. The amount of O_2 adsorbed at 298 K corresponds to one monolayer of PdO. No further uptake of O_2 is observed until 473 K, the
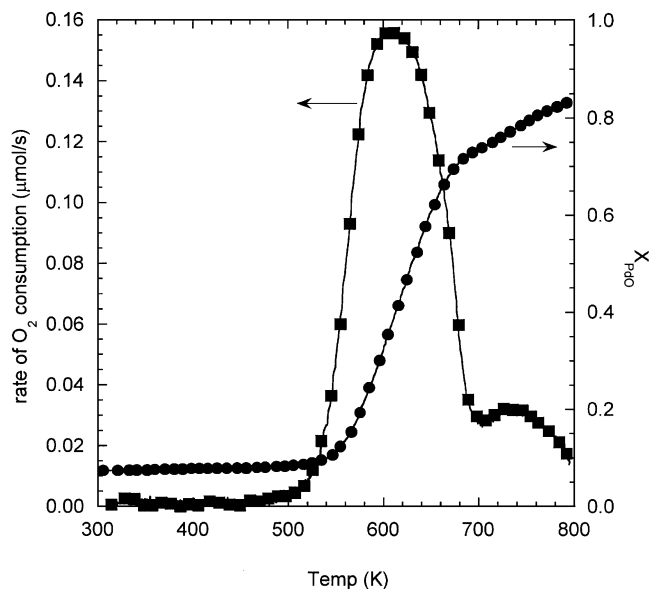
FIG. 3. Temperature programmed oxidation profile and oxygen content of 10 wt% Pd/ZrO$_2$.

threshold for bulk oxidation of Pd (31). Above 473 K, the oxidation of Pd proceeds very rapidly, reaching a maximum at 600 K. By 700 K, the rate of oxidation has slowed down considerably, but only 70% of the Pd has been converted to PdO. Raising the temperature further results in the appearance of a second peak at 740 K. The TPO experiment was terminated at 800 K, at which point 85% of the Pd had been converted to PdO. The physical significance of the two TPO peaks is discussed below. From a plot of the natural logarithm of the rate of oxidation for the onset of bulk oxidation versus 1/T, the activation

energy for the initial bulk oxidation of Pd is estimated to be 100 kJ/mol.

The dynamics of Pd oxidation were also investigated under isothermal conditions. In this case, a mixture containing 5% O_2 in He flowing at 60 cm^3/min was passed over the sample. The extent of Pd oxidation was measured after a fixed period of time by measuring the total amount of CO_2 released upon TPR of the sample in CH_4. *In situ* Raman measurements were also made to determine the extent to which the intensity of the band at 651 cm^{-1} tracks the formation of PdO. Results are shown in Fig. 4 for temperatures
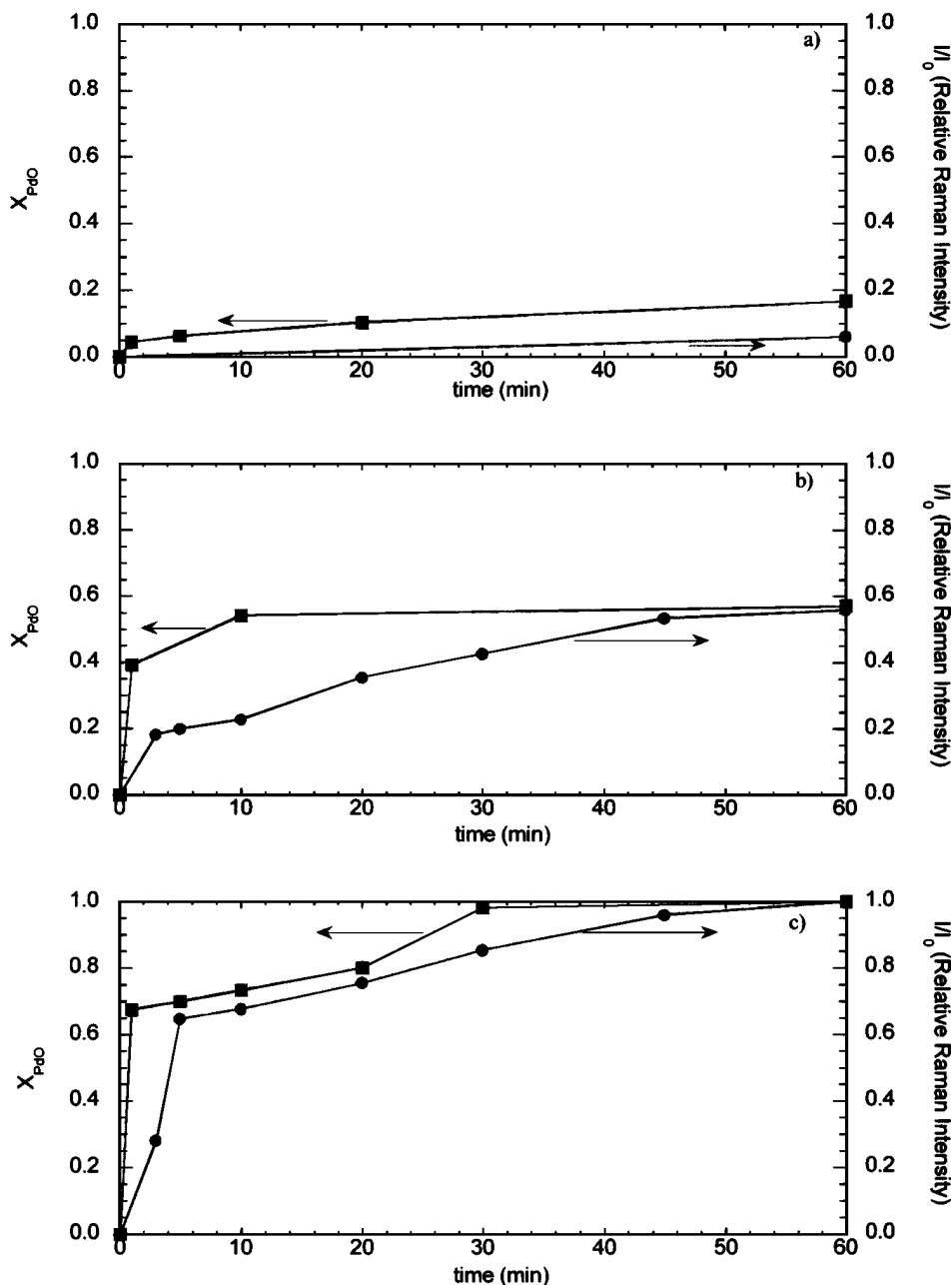
FIG. 4. Oxygen content and relative Raman intensity of 10 wt% Pd/ZrO$_2$ during isothermal oxidation in 1 atm 5% O$_2$/He at (a) 533 K, (b) 673 K, and (c) 773 K.

of 533, 673, and 773 K. At each temperature, the extent of oxidation rises very rapidly during the first minute of oxidation and then proceeds much more slowly thereafter. The amount of oxidation during the first minute is $x_{PdO} = 0.05$, 0.40, and 0.68 for temperatures of 533, 673, and 773 K, respectively, and the corresponding values after 1 h of oxidation are $x_{PdO} = 0.15$, 0.55, and 1.0. The observed pattern of oxidation is similar that reported previously for Pd/Al_2O_3 (2) and Pd films (16).

The dynamics of Pd oxidation are characteristic of those expected for metal oxidation in the thin-film (oxide thickness <15 nm) regime occurring in accordance with the Cabrera–Mott theory (32). Electrons from the metal are assumed to tunnel through the thin oxide layer (L(t)) and react with adsorbed oxygen atoms to form oxygen anions. The velocity of the electrons is considered to be much higher than for the oxygen anions, so that charge separation occurs across the oxide film, creating an electrostatic potential (V_M) between the oxygen-oxide and oxide metal interfaces. The surface-charge electric field ($E_o = V_M/L(t)$) then drives the anions towards the oxide–metal interface. Because the field is inversely proportional to the oxide film thickness, oxidation is initially very rapid and then sharply levels off to a very slow growth rate. During this latter phase, the rate of oxygen transport to the oxide–metal interface is progressively dominated by diffusion. Accordingly, we ascribe the very rapid growth in PdO during the first minute of oxidation to electric-field driven oxidation (i.e., the Cabrera–Mott mechanism), whereas the slower subsequent rate of PdO accumulation is likely limited by the diffusion of oxygen atoms through the earlier deposited PdO film. In a similar manner, it is believed that the first of the two TPO peaks observed in Fig. 3 is due to Pd oxidation via the Cabrera–Mott mechanism, while the second peak is due to diffusion-limited oxidation of Pd.

The relative intensity of the Raman band at 651 cm^{-1} follows a time evolution that is qualitatively similar to that exhibited by x_{PdO}, but always lags the latter quantity (see Fig. 4). However, the gap between the values of x_{PdO} and I/I_0 decreases with increasing temperature. This pattern can be explained by suggesting that the PdO film formed on the surface of the Pd particles is partly amorphous and partly crystalline. If the Raman scattering cross section for the crystalline phase is larger than that for the amorphous phase, then the intensity of the Raman signal would reflect the fraction of the PdO that is crystalline. Such an interpretation would be consistent with the observation that during the initial phase of Pd oxidation an amorphous film forms which then slowly undergoes crystallization. The transformation of an amorphous film to a crystalline oxide has been observed for a number of situation involving metal oxidation, and increasing the temperature has been shown to accelerate the rate at which the amorphous phase is converted to the crystalline phase (32). The disparity between

Raman intensity and extent of oxidation seen in Fig. 4 has also been observed during oxidation of a Pd film (16). For oxide thicknesses between 0.7 and 5.7 nm, while the thickness increased eightfold, the Raman intensity increased by over a factor of 100. Only for oxide thicknesses greater than 10 nm did the Raman intensity increase linearly with the extent of oxidation.

Additional information about the types of oxide formed during oxidation is obtained from inspection of TPR spectra taken after progressively greater degrees of oxidation. Figure 5 shows a series of TPD spectra taken during the reduction of PdO in CH_4. In such experiments the only products formed are CO_2 and H_2O. After oxygen uptake at 373 K for 30 min on a fully reduced sample of Pd/ZrO_2, a single broad feature is observed between 520 and 750 K. The amount of O_2 adsorbed corresponds to 1 ML of Pd. This peak, centered at 620 K, is attributed to the reduction of atomically adsorbed O on the surface of Pd. As the temperature of oxygen uptake increases, a new peak appears at about 560 K which overlaps the surface-oxide peak. This feature is ascribed to the reduction of subsurface oxide.
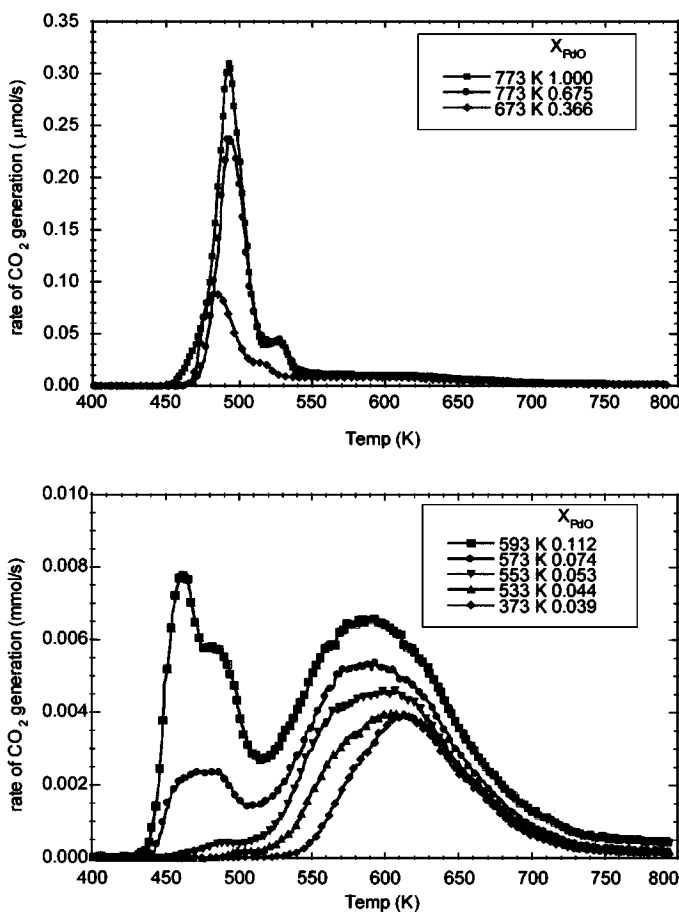
FIG. 5. Temperature programmed reduction of 10 wt% Pd/ZrO_2 in 1 atm 3% CH_4/He following oxidation in 1 atm 5% O_2/He at different temperatures.

When the extent of oxidation exceeds $x_{PdO} = 0.05$, a pair of overlapping peaks become evident at 460 and 480 K. Increasing the extent of oxidation above $x_{PdO} = 0.3$ causes these latter peaks to shift to higher temperature and then stabilize at 480 and 530 K. Based on the amount of oxygen associated with these low temperature features, they are attributed to the reduction of bulk PdO. The upward shift in temperature of these peaks with increasing temperature of oxidation may reflect a growing proportion of crystalline PdO in the deposited oxide layer.

The dynamics of PdO reduction were further explored in a series of isothermal reduction experiments. A fully oxidized sample of Pd/ZrO$_2$ was exposed to a mixture containing 3% CH$_4$ in He flowing at 60 cm^3/min, and the rate of PdO oxidation determined by monitoring the evolution of CO$_2$. As seen in Fig. 6, PdO reduction is preceded by a period of induction during which no CO$_2$ is formed, after which the rate of reduction rises and then passes through a maximum. An experiment conducted at 423 K revealed that neither CO$_2$ nor H$_2$O acumulate on the catalyst during the induction period. With increasing temperature, the induction period decreases and the maximum shifts to shorter times. Plotting the data as the natural logarithm of the rate of CO$_2$ formation versus x_{Pd} (i.e., $1 - x_{PdO}$) produces the plots shown in Fig. 6. It is observed that following a very rapid rise in the rate of PdO reduction, the rate of PdO reduction is nearly independent of x_{Pd}.

The observed dependencies of the rate of reduction on time and the extent of reduction (Fig. 6) are characteristic of nucleation-controlled reduction, in which small nuclei of metal must first form before the rest of the oxide can undergo rapid reduction (33). This would suggest that the
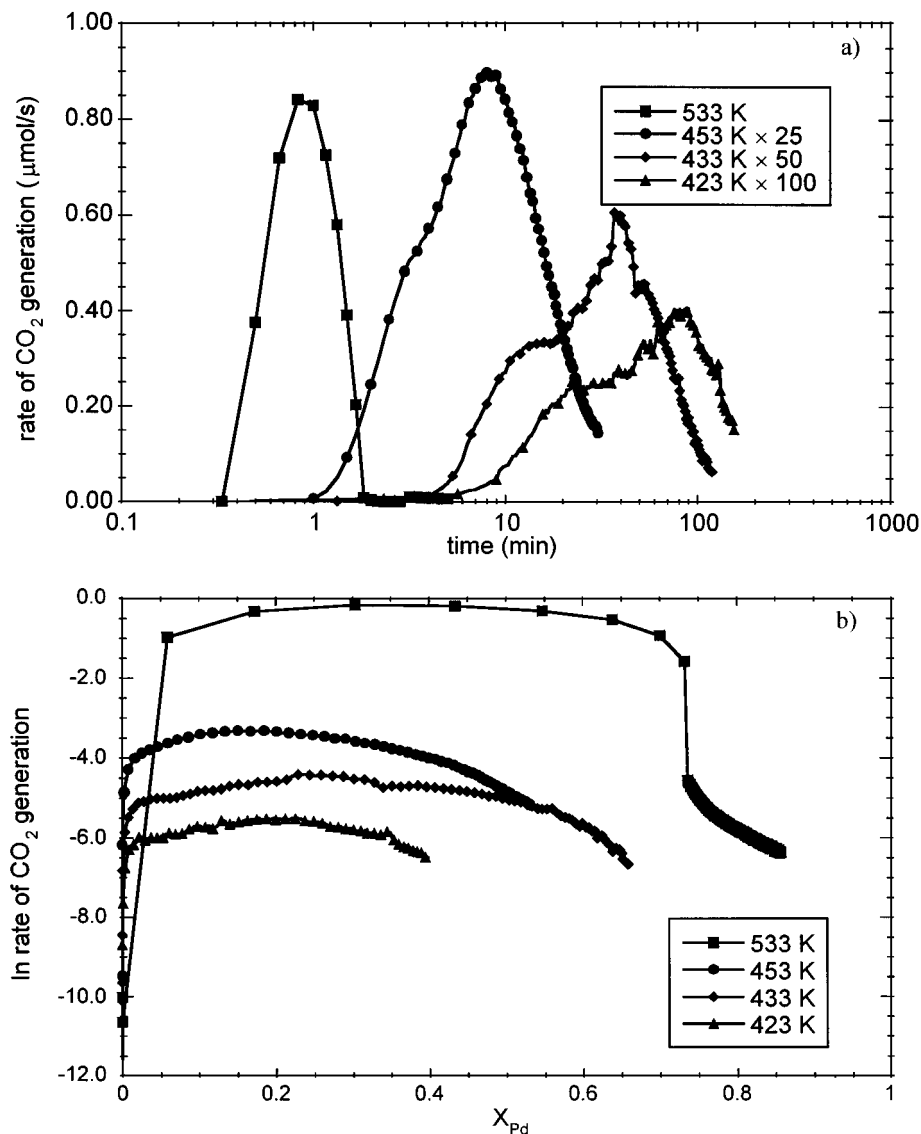
FIG. 6. Isothermal reduction of 10 wt% Pd/ZrO$_2$ in 1 atm 3% CH$_4$/He with (a) time and (b) extent of reduction.
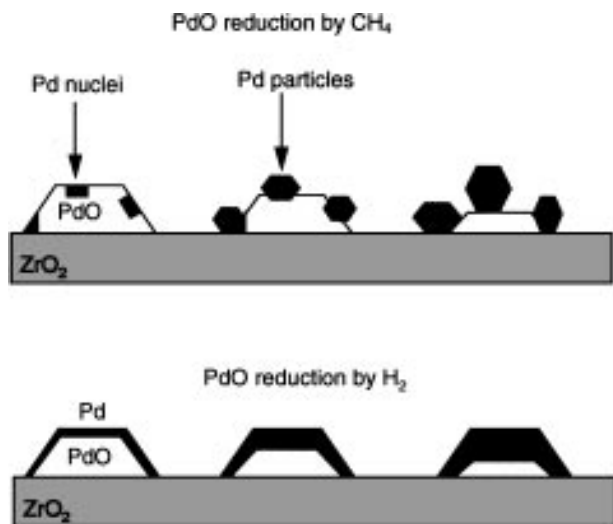
FIG. 7. Illustrations of nucleated reduction of PdO by CH_4 and shell-wise reduction of PdO by H_2.

dissociative adsorption of CH_4 occurs more effectively on metallic Pd than on bulk PdO, and that once formed the fragments of the dissociative adsorption of CH_4 (viz, CH_3 and H), spill over onto the oxide and rapidly reduce it. The near zero-order dependence of the reduction rate on x_{Pd} suggests that reduction may occur along a fixed line of contact between the oxide and the metal particles, which detach from the oxide surface in the manner illustrated schematically in Fig. 7.

Further insights into the dynamics of PdO reduction were obtained from Raman spectra taken during the course of PdO reduction. Figure 8 shows plots of x_{PdO} and the relative intensity of the band at 651 cm^{-1} versus time. At 473 K, the two sets of data are nearly parallel to each other, but as the temperature rises, the intensity of the Raman signal falls more rapidly than does x_{PdO} with time. This trend can be attributed to the accumulation of Pd particles on the surface of PdO as reduction proceeds. Since Pd particles will adsorb and scatter the incident laser radiation used for Raman spectroscopy, the more metallic Pd accumulated on the surface of the PdO, the harder it will be to record a spectrum of PdO. An extreme case of this phenomenon is observed when H_2 is used to reduce the sample. As shown in Fig. 9, removal of only 5% of the PdO results in the complete loss of the Raman signal from the remaining 95% of the PdO. The effect is dramatic because H_2 reduces the surface of the PdO so quickly that it occurs in a shellwise fashion. The deposited Pd shell acts as an effective screen for the laser radiation of the Raman spectrometer, making it impossible to probe the oxide layer lying below the metal film. Interestingly, if the reduced sample is annealed in He at 673 K for 30 min, the intensity of the Raman band at 651 cm^{-1} is restored because oxygen in the bulk of the particles oxidizes the thin film of Pd covering the particle.

By contrast, when 5% of the PdO is removed with CH_4 at 473 K, the Raman scattering is still able to observe nearly 84% of the remaining PdO. Only during more rapid reductions in CH_4 at 533 K does the Pd significantly block the laser radiation from the remaining PdO.

The impact of metallic Pd on the reduction of PdO is shown in Fig. 10. When approximately 15% of the initial inventory of PdO is removed by reduction at 533 K with pulses of CH_4, the induction period is reduced and the initial rate of reduction is increased. By contrast, removal of 15% of the initial inventory of PdO by reduction at 533 K with pulses of H_2 increases the induction time substantially relative to that observed for the fully oxidized sample. These results clearly show that the nature of the reducing agent has a profound effect on the dynamics of PdO reduction by CH_4 following the initial period of reduction. The patterns seen in Fig. 10 can be interpreted in the following way. In the case of prereduction in CH_4, the particles of Pd are separated from the surface of the remaining PdO (see Fig. 7), so that access to the surface of the oxide is possible for the fragments formed upon dissociative adsorption of CH_4 on the metal particles. However, after prereduction in H_2, a shell of Pd covers the surface of the oxide (see Fig. 7). As a consequence, access to the remaining PdO by the fragments of CH_4 dissociation is limited to grain boundaries and defects in the metal overlayer, and the onset of reduction in CH_4 is severely retarded.

The effects of progressive prereduction by CH_4 and H_2 are illustrated in Figs. 11a and b. In both cases prereduction was carried out by passing pulses of the reducing agent over a fully oxidized sample held at 533 K. It is evident from the TPR spectra shown in Fig. 11a that prereduction in CH_4 enhances the initial rate of reduction in CH_4 when the temperature is ramped at 10 K/min (see inset). Annealing of an initially prereduced sample in He at 533 K for 30 min causes an increase in the temperature required to achieve a given rate of reduction in CH_4. This effect is particularly evident in the low-temperature portion of the TPR spectrum shown in the inset of Fig. 11a and is believed to be due to the diffusion of oxygen from the oxide to the segregated Pd particles (see Fig. 7) to produce a relatively reduction-resistant oxide monolayer. Prereduction in H_2 has exactly the opposite effect to that of CH_4. Figure 11b shows that with increasing prereduction, the initial rate of PdO reduction declines monotonically. What is particularly interesting in this case is the observation that prereduction of PdO in H_2 and subsequent annealing of the sample at 533 K in He for 30 min increases the initial rate of reduction in CH_4 relative to that observed without annealing. Two explanations can be offered. The first is that annealing causes partial sintering of the Pd overlayer, with consequent increase in the amount of PdO surface area accessible for reduction by the fragments of the dissociative adsorption of CH_4 on Pd. The second interpretation is that annealing brings
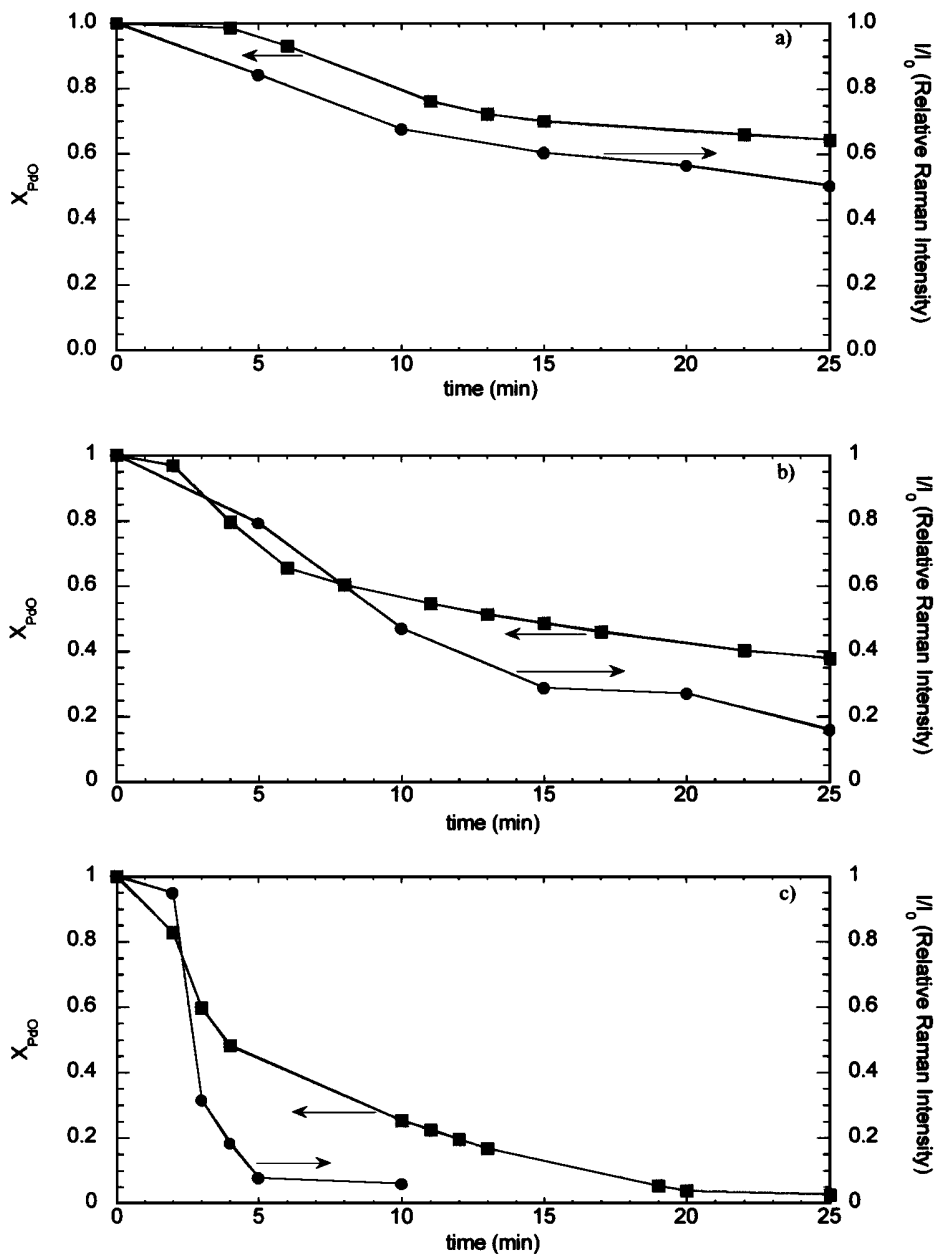
FIG. 8. Oxygen content and relative Raman intensity of 10 wt% Pd/ZrO$_2$ during isothermal reduction in 1 atm 3% CH$_4$/He at (a) 473 K, (b) 503 K, and (c) 533 K.

oxygen to the surface of the Pd film covering the surface of the residual PdO, by means of diffusion of atomic oxygen through the Pd film.

The results presented in Figs. 6, 8, and 9 clearly demonstrate that metallic Pd is needed to nucleate the reduction of PdO by CH$_4$. A recent study has shown that CH$_4$ will adsorb dissociatively on metallic Pd at temperatures above 400 K (26). The CH$_x$ (x = 3–1) species and H atoms thus formed are assumed to diffuse to the Pd/PdO interface and initiate the reduction of PdO. Consistent with this picture, recent studies conducted with Pd(110) (27) have shown that

dissociative adsorption of CH$_4$ occurs on Pd, but is progressively inhibited by the presence of adsorbed oxygen, the sticking coefficient for dissociative adsorption decreasing linearly with increasing oxygen coverage. The preference of metallic Pd for the dissociation of CH$_4$ is also supported by recent quantum chemical calculations (34–37).

The results in Fig. 6 can be used to calculate an activation energy for the induction period, the initial rate of reduction of fully oxidized PdO, and the reduction rate for partially oxidized PdO, when PdO is reduced by CH$_4$. For the induction period, the nucleation process is assumed to be first
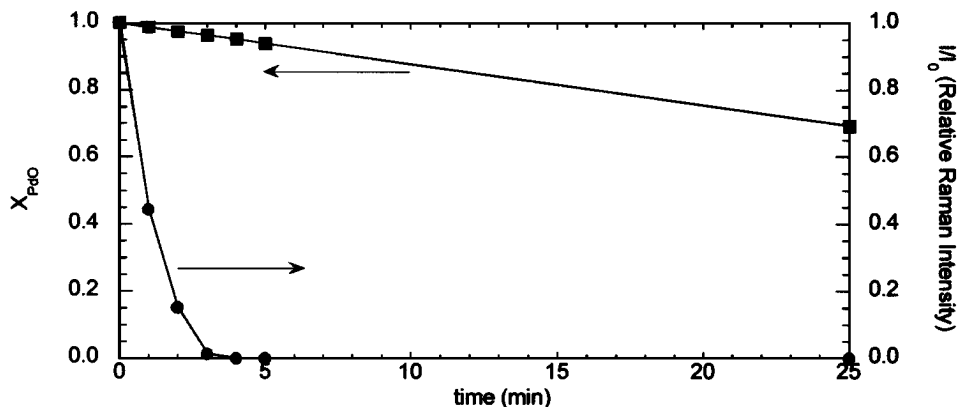
FIG. 9. Oxygen content and relative Raman intensity of 10 wt% Pd/ZrO$_2$ during isothermal reduction in 1 atm 0.2% H$_2$/He at 533 K.

order,

$$dN/dt = k_0 \exp(-E_a/RT), \qquad [1]$$

where N is the number of nuclei. This equation can be integrated from $t = 0$, for which it assumed that $N = 0$, to the length of the induction period, t_i, at which point the number of nuclei are assumed to have reached some critical number, N_c. The apparent activation energy of 89 kJ/mol for the induction period can be obtained by plotting $\ln(1/t_i)$ versus $1/T$.

For the initial rate of reduction when less than 1 ML of PdO has been reduced, the rate expression is assumed to have the form

$$d[CO_2]/dt = k_0 \exp(-E_a/RT)(\theta_{Pd}). \qquad [2]$$
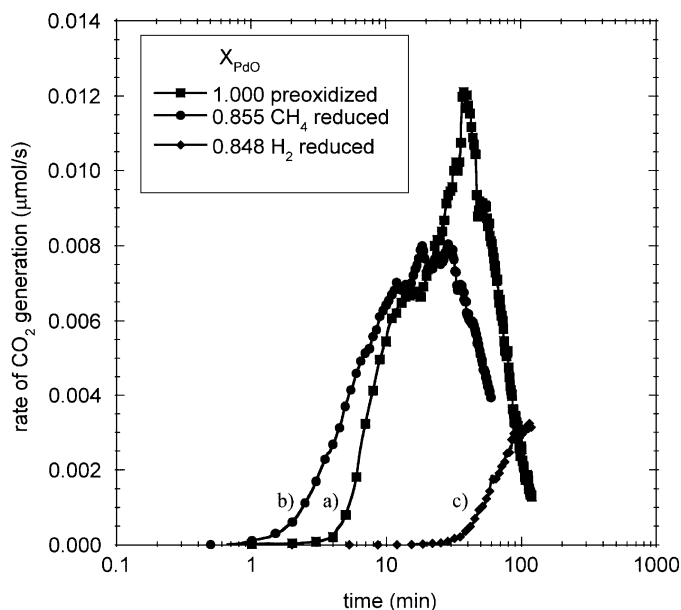
A plot of $\ln(d[CO_2]/dt)$ versus $\ln(\theta_{Pd})$ has a slope of approximately 1, indicating that the initial rate of reduction is first order in Pd surface concentration, as postulated. The corresponding activation energy is found to be 97 kJ/mol. Figure 6 shows that after the initial rate increase, the reduction rate becomes nearly independent of x_{Pd} for values of x_{Pd} between 0.04 and 0.30. It is believed that the metal/metal oxide interface is approximately constant during this stage of the reduction. With the assumptions of a zeroth order rate of reduction in Pd, the apparent activation energy for reduction of PdO for $x_{Pd} = 0.04–0.3$ can be obtained from the Arrhenius plot. In this regime, the activation energy for reduction by CH$_4$ rises to 119 kJ/mol. An identical value was obtained from an analysis of the shift in the peak position as a function of heating for a series of TPR experiments (38).

CONCLUSIONS

The oxidation of fully reduced Pd/ZrO$_2$ proceeds through several stages. Oxygen is dissociatively adsorbed on the surface of the Pd particles forming a monolayer of adsorbed O. Above 473 K, oxidation of the bulk is initiated. This process involves the formation of an amorphous oxide layer which then transforms into crystalline PdO. The dynamics of oxidation are qualitatively consistent with that expected for metal oxidation occurring via the Cabrera–Mott theory. Very rapid oxidation occurs as a consequence of electric field-driven transport of oxygen anions through the oxide film. Once the film thickness exceeds about 15 nm, oxidation occurs more slowly via diffusive transport of oxygen through the oxide film. The reduction of PdO by H$_2$ and CH$_4$ occurs by different mechanisms. In the case of H$_2$, H$_2$ occurs rapidly and reduces the oxide in a shellwise manner. If the shell is kept thin, oxygen can diffuse through the metal layer and reoxidize it. Methane does not readily dissociate on PdO, and hence, an induction period is observed before rapid reduction occurs. During the induction period, small particle of metallic Pd form and segregate from the PdO surface. After the initial phase of reduction during

FIG. 10. Isothermal reduction of 10 wt% Pd/ZrO$_2$ in 1 atm 3% CH$_4$/He after (■) full preoxidation, (●) partial reduction in H$_2$, and (◆) partial reduction in CH$_4$.
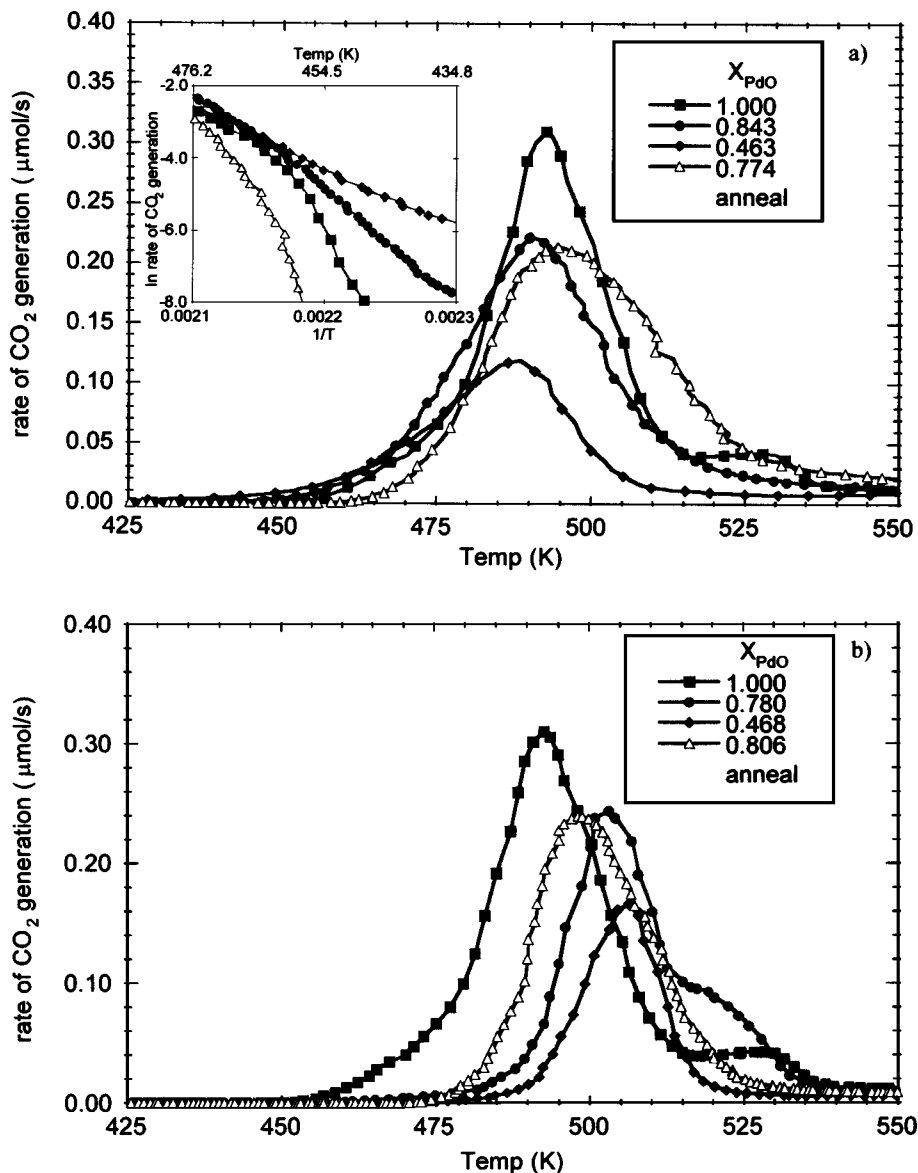
FIG. 11. Temperature programmed reduction of 10 wt% Pd/ZrO$_2$ in 1 atm 3% CH$_4$/He following (a) partial reduction in CH$_4$ and (b) partial reduction in H$_2$.

which the rate of reduction is first order in the amount of Pd formed, the rate of reduction becomes zero order in metallic Pd. This pattern suggests that once the particles of Pd separate from the PdO surface, the area of attachment between the Pd particle and the PdO remains constant and further reduction occurs at the metal–oxide boundary. Thus, it is evident that the reduction of PdO by methane occurs via a nucleation mechanism and requires the presence of metallic Pd.

ACKNOWLEDGMENTS

REFERENCES

1. Lee, J. H., and Trimm, D. L., *Fuel Processing Tech.* **42**, 339 (1995).
2. Burch, R., and Urbano, F. J., *Appl. Catal. A* **124**, 121 (1995).
3. Carstens, J. N., Su, S. C., and Bell, A. T., *J. Catal.* **176**, 136 (1998).
4. Orent, T. W., and Bader, S. D., *Surf. Sci.* **115**, 323 (1982).
5. Stuve, E. M., and Madix, R. J., *Surf. Sci.* **146**, 155 (1984).
6. Chang, S.-L., and Thiel, P. A., *J. Chem. Phys.* **88**, 2071 (1988).
7. Peuckert, M., *J. Phys. Chem.* **89**, 2481 (1985).
8. Guo, X., Hoffman, A., and Yates, J. T., Jr., *J. Chem. Phys.* **90**, 5787 (1989).

9. Imbihl, R., and Demuth, J. E., *Surf. Sci.* **173**, 395 (1986).
10. Conrad, H., Ertl, G., Kuppers, J., and Latta, E. E., *Surf. Sci.* **65**, 245 (1977).
11. Banse, B. A., and Koel, B. E., *Surf. Sci.* **232**, 275 (1990).
12. Weissman, D. L., Shek, M. L., and Spicer, W. E., *Surf. Sci.* **92**, L59 (1980).
13. Weissman-Wenocur, D. L., Shek, M. L., Stefan, P. M., Lindau, I., and Spicer, W. E., *Surf. Sci.* **127**, 513 (1983).
14. Légaré, P., Hilaire, L., Maire, G., Krill, G., and Amamou, A., *Surf. Sci.* **107**, 533 (1981).
15. Campbell, C. T., Foyt, D. C., and White, J. M., *J. Phys. Chem.* **81**, 491 (1977).
16. Remillard, J. T., Weber, W. H., McBride, J. R., and Soltis, R. E., *J. Appl. Phys.* **71**, 4515 (1992).
17. Chen, J. J., and Ruckenstein, E., *J. Phys. Chem.* **85**, 1606 (1981).
18. Ruckenstein, E., and Chen, J. J., *J. Colloid Interface Sci.* **86**, 1 (1982).
19. Otto, K., Hubbard, C. P., Weber, W. H., and Graham, G. W., *Appl. Catal. B* **1**, 317 (1992).
20. Engel, T., and Kuipers, H., *Surf. Sci.* **90**, 181 (1979).
21. Nyberg, C., and Tengstål, C. G., *Surf. Sci.* **126**, 163 (1983).
22. Müller, C. A., Maciejewski, M., Koeppel, R. A., Tschan, R., and Baiker, A., *J. Phys. Chem.* **100**, 20006 (1996).
23. Hicks, R. F., Qi, H., Young, M. L., and Lee, R. G., *J. Catal.* **122**, 295 (1990).
24. McCarty, J. G., *Catal. Today* **26**, 283 (1995).
25. König, D., Weber, W. H., Poindexter, B. D., McBride, J. R., Graham, G. W., and Otto, K., *Catal. Lett.* **29**, 329 (1994).
26. Solymosi, F., Erdöhelyi, A., Cserényi, and Felvégi, *J. Catal.* **147**, 272 (1994) and references therein.
27. Valden, M., Pere, J., Xiang, N., and Pessa, M., *Chem. Phys. Lett.* **257**, 289 (1996).
28. Benson, J. E., Hwang, H. S., and Boudart, M., *J. Catal.* **30**, 146 (1973).
29. Weber, W. H., Baird, R. J., and Graham, G. W., *J. Raman Spectrosc.* **19**, 239 (1988).
30. McBride, J. R., Haas, K. C., and Weber, W. H., *Phys. Rev. B* **44**, 5016 (1991).
31. Lam, Y. L., and Boudart, M., *J. Catal.* **47**, 393 (1977).
32. Fromhold, A. T., *Theory of Metal Oxidation Volume 1-Fundamentals* (North-Holland, Amsterdam, 1976), p. 7.
33. Hurst, N. W., Gentry, S. J., Jones, A., and McNicol, B. D., *Catal. Rev. Sci. Eng.* **24**, 233 (1982).
34. Blomberg, M. R. A., Siegbahn, P. E. M., and Svensson, M., *J. Phys. Chem.* **98**, 2062 (1994).
35. Blomberg, M. R. A., Siegbahn, P. E. M., and Svensson, M., *J. Phys. Chem.* **96**, 5783 (1992).
36. Broclawik, E., Yamauchi, R., Endou, A., Kubo, M., and Miyamoto, A., *J. Chem. Phys.* **104**, 4098 (1996).
37. Broclawik, E., Yamauchi, R., Endou, A., Kubo, M., and Miyamoto, A., *Int. J. Quan. Chem.* **61**, 673 (1997).
38. Falconer, J. L., and Schwarz, J. A., *Catal. Rev.-Sci. Eng.* **25**, 141 (1983).